



1 **Impact of buildings on surface solar radiation over urban**
2 **Beijing**

3 **B. Zhao¹, K. N. Liou¹, Y. Gu¹, C. He¹, W. L. Lee², X. Chang³, Q. B. Li¹, S. X. Wang³,**
4 **⁴, H. R. Tseng¹, L. R. Leung⁵, J. M. Hao^{3, 4}**

5 [1] Joint Institute for Regional Earth System Science and Engineering and Department of
6 Atmospheric and Oceanic Sciences, University of California, Los Angeles, CA 90095, USA

7 [2] Research Center for Environmental Changes, Academia Sinica, Taipei, Taiwan

8 [3] State Key Joint Laboratory of Environment Simulation and Pollution Control, School of
9 Environment, Tsinghua University, Beijing 100084, China

10 [4] State Environmental Protection Key Laboratory of Sources and Control of Air Pollution
11 Complex, Beijing 100084, China

12 [5] Pacific Northwest National Laboratory, Richland, WA 99352, USA

13
14 Correspondence to: B. Zhao [zhaob1206@gmail.com]

15
16 **Abstract.**

17 The rugged surface of an urban area due to varying buildings can interact with solar beams
18 and affect both the magnitude and spatiotemporal distribution of surface solar fluxes. Here we
19 systematically examine the impact of buildings on downward surface solar fluxes over urban
20 Beijing by using a 3-D radiation parameterization that accounts for 3-D building structures
21 versus the conventional plane-parallel scheme. We find that the resulting downward surface
22 solar flux deviations between the 3-D and the plane-parallel schemes are generally ± 1 –
23 10 W m^{-2} at 800-m grid resolution and within $\pm 1 \text{ W m}^{-2}$ at 4-km resolution. Pairs of positive-
24 negative flux deviations on different sides of buildings are resolved at 800-m resolution, while
25 they offset each other at 4-km resolution. Flux deviations from the unobstructed horizontal
26 surface at 4-km resolution are positive around noon but negative in the early morning and late
27 afternoon. The corresponding deviations at 800-m resolution, in contrast, show diurnal
28 variations that are strongly dependent on the location of the grids relative to the buildings.
29 Both the magnitude and spatiotemporal variations of flux deviations are largely dominated by
30 the direct flux. Furthermore, we find that flux deviations can potentially be an order of
31 magnitude larger by using a finer grid resolution. Atmospheric aerosols can reduce the



1 magnitude of downward surface solar flux deviations by 10–65%, while the surface albedo
2 generally has a rather moderate impact on flux deviations. The results imply that the effect of
3 buildings on downward surface solar fluxes may not be critically significant in mesoscale
4 atmospheric models with a grid resolution of 4 km or coarser. However, the effect can play a
5 crucial role in meso-urban atmospheric models as well as microscale urban dispersion models
6 with resolutions of 1 m – 1 km.

8 **1 Introduction**

9 The spatial orientation and inhomogeneous features of the earth's surface interact with direct
10 and diffuse solar beams in an intricate manner (Liou et al., 2013). In particular, the complex
11 and rugged surface of an urban area due to varying buildings can interact with solar beams
12 and affect both the magnitude and spatiotemporal distribution of surface solar fluxes. The
13 distribution of solar fluxes can significantly modulate surface heating and moistening,
14 evapotranspiration, land-atmosphere interaction, boundary layer, and air pollutant dispersion
15 (Lee et al., 2011; Gu et al., 2012). It is very difficult to accurately quantify the surface solar
16 flux distribution in view of the complexity of spatial orientation and surface optical properties,
17 especially over urban areas.

18 Several approaches with varying degrees of sophistication have been developed to evaluate
19 solar fluxes at rugged surface (Dozier and Frew, 1990; Dubayah et al., 1990; Chen et al., 2006;
20 Essery and Marks, 2007; Lai et al., 2010). Among these approaches, the 3-D Monte Carlo
21 photon tracing approach gives the most physically-representative radiative transfer
22 calculations for an environment with complex 3-D topography. Chen et al. (2006) and Liou et
23 al. (2007) developed a Monte Carlo program and found that the domain-average downward
24 surface solar fluxes with rugged topography deviate from the unobstructed horizontal surface
25 by 10–50 W m⁻² over the Tibetan Plateau and can be as large as 600 W m⁻² locally over
26 shaded areas. The 3-D Monte Carlo approach has also been used to evaluate interactions
27 between solar beams and other irregular surfaces, such as wind-blown sea surfaces and plant
28 canopies (Preisendorfer and Mobley, 1986; Iwabuchi and Kobayashi, 2008; Mayer et al.,
29 2010). However, a drawback of the 3-D Monte Carlo photon tracing approach is the enormous
30 computational burden. To overcome this drawback, Lee et al. (2011, 2013) developed a
31 parameterization of downward solar fluxes associated with topographic information based on
32 3-D Monte Carlo simulations. The parameterization was subsequently implemented in



1 regional and global weather and climate models (Liou et al., 2013; Lee et al., 2015; Gu et al.,
2 2012) in which the effects of 3-D mountainous topography on sensible and latent heat fluxes,
3 surface hydrology, and cloud properties have been investigated and evaluated.

4 With the objective to improve the urban representation in land-surface schemes that has
5 been used in numerical models, a number of urban energy balance models (or urban canopy
6 models) have been developed, as reviewed by Grimmond et al. (2010, 2011). Some of these
7 models have considered a building's shading effect and the reflectance of solar beams by
8 building walls (Kusaka et al., 2001; Kusaka and Kimura, 2004; Kondo et al., 2005; Oleson et
9 al., 2008). However, these models have at least two drawbacks. First, the 3-D radiative
10 transfer was calculated based on simplified, evenly spaced buildings of the same height, rather
11 than "real" buildings. Second, the diffuse, diffuse-reflected, and coupled fluxes (e.g., multiple
12 reflections) were often oversimplified, resulting in noticeable errors due to the distinct
13 features of the different flux components. A systematic evaluation and physical understanding
14 of the 3-D building effect on surface solar radiation over urban areas is imperative.

15 In this study, we investigate the impact of buildings on downward surface solar fluxes over
16 urban Beijing, the capital and one of the largest megacities in China. The evaluation is
17 conducted using the 3-D radiation parameterization developed by Lee et al. (2013) coupled
18 with the Fu-Liou-Gu (FLG) plane-parallel radiative transfer scheme (Fu and Liou, 1992; Gu
19 et al., 2003; Gu et al., 2006). In Section 2, we describe the parameterization of 3-D
20 topography effect on downward solar fluxes and its application over urban Beijing. In Section
21 3, we investigate the magnitude and spatiotemporal variation of deviations in downward
22 surface solar fluxes induced by buildings and evaluate the effect of key factors by means of
23 sensitivity simulations. Conclusions and implications are given in Section 4.

24 **2 Methodology and data source**

25 **2.1 Parameterization of the 3-D topography effect on downward surface solar** 26 **fluxes**

27 In order to evaluate the impact of buildings on downward surface solar radiation, we apply the
28 3-D radiation parameterization over rugged surface developed by Lee et al. (2013). Below are
29 key points of the parameterization. Note that we focus exclusively on "downward" solar
30 fluxes in this study.



1 Solar radiative fluxes can be categorized into five components according to photon path: (1)
 2 direct flux (F_{dir}) is composed of photons hitting the ground directly from the sun without
 3 encountering scattering or reflection; (2) diffuse flux (F_{dif}) contains photons experiencing
 4 single or multiple scattering by air molecules, but does not encounter surface reflection; (3)
 5 direct-reflected flux (F_{rdir}) is comprised of unscattered photons reflected by nearby terrain;
 6 (4) diffuse reflected flux (F_{rdif}) means that photon is first scattered by air molecules and then
 7 reflected by nearby terrain; and (5) coupled flux (F_{coup}) represents photons that after being
 8 reflected by the surface, encounter scattering and/or one or more additional surface
 9 reflections.

10 Conventional plane-parallel radiative transfer schemes have already been developed to
 11 calculate solar fluxes on a horizontal surface, so the purpose of the 3-D radiation
 12 parameterization is to produce relative deviations of these five flux components from those of
 13 an unobstructed horizontal surface. On the basis of 3-D Monte Carlo photon tracing
 14 simulations, Lee et al. (2011, 2013) utilized a multiple linear regression technique to establish
 15 the relationship between deviations in solar fluxes (response variables) and subgrid scale
 16 topographic information (independent variables). The Shuttle Radar Topography Mission
 17 (SRTM) topography data (Jarvis et al., 2008) at a resolution of 3 arc-second (about 90 m)
 18 were used to perform 3-D Monte Carlo simulations for many $10 \times 10 \text{ km}^2$ rugged domains in
 19 the Sierra Nevada Mountain area, which were subsequently used to develop regression
 20 parameterization. Although the parameterization was developed in the Sierra Nevada area, it
 21 is applicable to other regions because it is topographic parameter-dependent rather than
 22 location-dependent. The regression equations for flux deviations in clear-sky condition can be
 23 expressed by

$$\begin{pmatrix} F'_{dir} \\ F'_{dif} \\ F'_{rdir} \\ F'_{rdif} \\ F'_{coup} \end{pmatrix} = \begin{pmatrix} a_1 \\ a_2 \\ a_3 \\ a_4 \\ a_5 \end{pmatrix} + \begin{pmatrix} b_{11} & b_{12} & 0 & 0 \\ b_{21} & b_{22} & 0 & b_{24} \\ 0 & b_{32} & b_{33} & 0 \\ 0 & b_{42} & b_{43} & 0 \\ b_{51} & b_{52} & b_{53} & 0 \end{pmatrix} \begin{pmatrix} \langle \tilde{\mu}_t \rangle \\ \langle \tilde{V}_d \rangle \\ \langle \tilde{C}_t \rangle \\ \sigma(h) \end{pmatrix}, \quad (1)$$

25 where F'_i is the relative deviation of each flux component, $i = dir, dif, rdir, rdif, \text{ and } coup$. a_i
 26 is the interception, b_{ij} is the regression coefficient for a specific independent variable. $\tilde{\mu}_t$ is



1 the cosine of the solar zenith angle normalized by the cosine of the slope, \tilde{V}_d is the sky view
2 factor normalized by the cosine of the slope, \tilde{C}_t is the terrain configuration factor normalized
3 by the cosine of the slope, $\sigma(h)$ is the standard deviation of elevation, and angle brackets
4 denote the spatial mean of the variable within a $10 \times 10 \text{ km}^2$ domain. Lee et al. (2013)
5 demonstrated that the flux components predicted by these regression equations agree well
6 with those directly calculated from Monte Carlo simulations.

7 **2.2 Application of the 3-D radiation parameterization to urban Beijing**

8 We apply the parameterization described above to Beijing, a megacity with numerous
9 buildings, many of which are skyscrapers. Two domains with different sizes and resolutions
10 are used (Fig. 1). Domain 1 covers urban and suburban Beijing at a grid resolution of 4 km,
11 which is a commonly used resolution in mesoscale atmospheric models. The Xishan mountain
12 is located in the northwestern part of the domain, serving as a comparison of the 3-D
13 topography effect over mountainous and urban areas. The rest of the domain is characterized
14 by plains with typical urban landscape (e.g., buildings and roads). Domain 2 covers the urban
15 center of Beijing at 800-m resolution, corresponding to the typical resolution of meso-urban
16 models.

17 Following Lee et al. (2013), we adopt the topography data at a resolution of 3 arc-second
18 (about 90 m) from SRTM, and calculate average topographical parameters for each 4 km or
19 800 m grid in the simulation domains. Figure 1 (right panel) shows that major buildings are
20 resolved in the 90 m topography data. The SRTM data is for the year 2000. We note that
21 urban development in Beijing has expanded greatly since 2000, far beyond what is
22 represented in the SRTM data. This study aims to assess the potential magnitude of the effect
23 of buildings on solar fluxes; the SRTM data meet the need considering that there were already
24 numerous buildings in Beijing in 2000.

25 The 3-D radiation parameterization was originally developed for $10 \times 10 \text{ km}^2$ grids. Lee et al.
26 (2011, 2013) demonstrated its compatibility across various resolutions. Theoretically it should
27 be applicable for a grid resolution as fine as 800 m since an $800 \times 800 \text{ m}^2$ grid still comprises a
28 large quantity of 90 m pixels. Here we further evaluate the compatibility associated with
29 resolutions by comparing the flux deviations in each $4 \times 4 \text{ km}^2$ grid calculated directly from the
30 3-D parameterization and those from the summation of all $800 \times 800 \text{ m}^2$ grids. We find the
31 biases between the two are within $\pm 0.025 \text{ W m}^{-2}$, indicating a reasonable compatibility



1 between different grid resolutions. The calculation method and subsequent results are
2 described in detail in the Supplementary Material.

3 The 3-D radiation parameterization is used in conjunction with the FLG plane-parallel
4 radiation scheme (Fu and Liou, 1992; Gu et al., 2003; Gu et al., 2006; Gu et al., 2010), which
5 calculates solar fluxes on flat surfaces. The FLG scheme combines the delta-four-stream
6 approximation for solar flux calculations with the delta-two/four-stream approximation for
7 infrared flux calculations to assure both accuracy and efficiency. The solar (0–5 μm) and
8 infrared (5–50 μm) spectra are divided into 6 and 12 bands, respectively, within which the
9 correlated k-distribution method is used to sort gaseous absorption lines. The single-scattering
10 properties of 18 aerosol types are parameterized by employing the Optical Properties of
11 Aerosols and Clouds (OPAC) database.

12 The meteorological and chemical variables (i.e., air temperature, surface temperature,
13 pressure, humidity, surface albedo, ozone concentrations, and aerosol optical depth) used in
14 the FLG scheme are derived from a simulation of the Weather Research and Forecasting
15 model (WRF, version 3.3)/Community Multi-scale Air Quality model (CMAQ, version 5.0.2).
16 The conversion of vertically resolved aerosol mass concentrations to aerosol optical depth
17 follows Heald (2010) and Martin and Heald (2010). For the WRF/CMAQ simulation, we
18 apply one-way, triple nesting domains with resolutions of 36 km, 12 km, and 4 km,
19 respectively (Fig. S1). The simulated meteorological parameters and concentrations of fine
20 particles (PM_{2.5}) and their chemical components are in reasonable agreement with
21 observations (Table S2, Fig. S2). The configuration of WRF/CMAQ and its evaluation against
22 observations are described in detail in the Supplementary Material. The meteorological and
23 chemical variables of Domain 1 (4-km resolution) are taken from the WRF/CMAQ simulation
24 directly, while the variables in Domain 2 (800-m resolution) are assumed to be the same as
25 their corresponding values at the 4 km grids.

26 The 3-D radiative transfer calculations are for January 1st, April 1st, July 1st, and October 1st,
27 2012, representing four seasons. Within each day, the calculation is done every hour starting
28 from 0:00, Beijing Time (BT). To avoid the fluctuation of atmospheric profiles, we conduct
29 the WRF/CMAQ simulations for four months (January, April, July, and October) and use
30 monthly average meteorological and chemical variables for each of the 24 hours in the 3-D
31 radiative transfer calculations. For example, for the simulation of January 1st 0:00 BT, we use
32 the average temperature at 0:00 BT of each day in January.



1 We conduct radiative transfer computation primarily for clear-sky condition without
2 aerosols, for which the 3-D radiation parameterization was developed. We also incorporate
3 aerosols for a sensitivity scenario (see Section 3.3.1). In the presence of aerosols, regression
4 equations for F'_{dir} and F'_{rdir} can be directly applied because these two components do not
5 encounter scattering. As for F'_{dif} , F'_{rdif} , and F'_{coup} , the parameterization provides a first-order
6 estimate (Lee et al., 2013; Lee et al., 2011). Considering that the direct flux usually dominates
7 over other components (Chen et al., 2006; Lee et al., 2011), the parameterization is likely
8 applicable in an environment with a large aerosol loading.

9 **3 Results and discussion**

10 **3.1 Deviations in solar fluxes from horizontal surface**

11 We calculate surface solar fluxes at rugged city surface by employing the 3-D radiation
12 parameterization coupled with the FLG plane-parallel scheme. Surface solar flux deviations
13 between the 3-D radiation parameterization and plane-parallel scheme represent the effect of
14 buildings. Figure 2 (top three rows) shows hourly flux deviations at selected times (7:00,
15 12:00, and 17:00 BT) on April 1st in clear-sky condition without aerosols. Figure 3 depicts
16 daily average flux deviations for four simulation days (January 1st, April 1st, July 1st, and
17 October 1st). For Domain 1 (4-km resolution), a striking feature is that deviations over urban
18 areas are remarkably smaller than those over mountainous areas. Both hourly and daily
19 average deviations over urban areas are generally within $\pm 1 \text{ W m}^{-2}$. In contrast, hourly/daily
20 average deviations over mountainous areas are on the order of $\pm 10\text{--}70 \text{ W m}^{-2}$, except for July
21 when daily average deviations are generally within 10 W m^{-2} . The maximum local deviations
22 can be up to $\pm 100 \text{ W m}^{-2}$. In Domain 2 (800-m resolution), both the magnitude and the spatial
23 pattern of deviations differ greatly from Domain 1. Flux deviations usually range between $\pm 1\text{--}$
24 10 W m^{-2} . The magnitude of flux deviations has a significant seasonal variation associated
25 with the position of the sun in different seasons. For example, daily average flux deviations
26 are within $\pm 10 \text{ W m}^{-2}$, $\pm 6 \text{ W m}^{-2}$, and $\pm 1 \text{ W m}^{-2}$ in January, April/October, and July,
27 respectively. Smaller daily average deviations in July are attributable to the smaller shading
28 effect at the north-south direction as the sun is close to its zenith at noon. In addition, the fine
29 structure of positive-negative pairs on southern-northern or eastern-western sides of buildings
30 is resolved in Domain 2. This phenomenon is especially pronounced when we compare flux
31 deviations at 7:00 BT and 17:00 BT. Many grids show opposite-sign flux deviations at these



1 two times, implying that they are located on the opposite side of buildings. The spatial pattern
2 comprising of positive-negative pairs is somewhat similar to that of mountainous areas in
3 Domain 1. By comparing Domain 1 and Domain 2, we conclude that flux deviations from the
4 flat surface over urban areas are quite sensitive to grid resolution. The magnitude of
5 deviations is small at a coarse resolution such as 4 km, because of the offset of positive and
6 negative deviations.

7 We further analyze the diurnal variation of flux deviations from the horizontal surface, as
8 shown in Fig. 4. To facilitate the analysis, we select a typical mountainous area (defined as
9 rectangle A in Fig. 1) and a typical urban area (defined as rectangle B in Fig. 1) in Domain 1,
10 as well as a typical urban area (defined as rectangle C in Fig. 1) in Domain 2. Flux deviations
11 in the typical urban area defined in Domain 1 (Fig. 4b) are positive during 6–7 hours around
12 noon with peaks occurring at noon, while they are negative in the early morning and late
13 afternoon. This diurnal pattern persists on all simulation days. At noon, buildings generally
14 receive more solar energy than a flat surface due to a larger surface area facing the sun,
15 whereas negative deviations in the early morning and late afternoon are primarily induced by
16 larger shading areas. The diurnal pattern over the typical urban area defined in Domain 2 (Fig.
17 4c) substantially differs from the preceding pattern such that flux deviations are positive in the
18 morning and negative in the afternoon. Figure 1 shows that these grids are mostly located in
19 the eastern side of the buildings rather than the western side. In this case, the eastern side
20 faces the sun in the morning, receiving more solar fluxes than its horizontal surface
21 counterpart. In the afternoon, the eastern side is shaded by the buildings to substantially block
22 solar beam. We note that the diurnal variation of grids in Domain 2 is a strong function of
23 their relative locations to the buildings. For example, the diurnal pattern is exactly opposite
24 for a grid containing more buildings' western side. Furthermore, it is noticeable that the
25 diurnal pattern of the typical urban area defined in Domain 2 highly resembles that of the
26 typical mountainous area defined in Domain 1 (Fig. 4a), which is located on the eastern side
27 of the Xishan mountain. This reveals the similarity between buildings and mountains in terms
28 of their impacts on surface radiation, though they are associated with different spatial scales –
29 4 km or more for mountains (Liou et al., 2013; Lee et al., 2013), and 800 m or less for
30 buildings.



1 **3.2 Contribution of individual flux components to flux deviations**

2 We quantify the contribution of individual flux components to surface solar flux deviations
3 between 3-D and plane-parallel in order to gain a deeper understanding of the effect of
4 buildings on solar flux distributions. Figure 5 shows the contribution of individual
5 components to flux deviations on April 1st in the three typical areas defined in the last section,
6 while Fig. S3 depicts the corresponding contributions on four simulation days (January 1st,
7 April 1st, July 1st, and October 1st) in the typical urban area defined in Domain 1. For the other
8 two typical areas, only April 1st is shown because the other simulation days present very
9 similar patterns. As described in Section 2.1, solar fluxes are physically categorized into five
10 components, including direct flux, diffuse flux, direct-reflected flux, diffuse-reflected flux,
11 and coupled flux. In Fig. 5, diffuse and coupled fluxes are merged together, considering that
12 the coupled flux is usually negligible and that these two components are treated together in the
13 plane-parallel scheme. A striking pattern is that the direct flux largely dominates deviations
14 from the unobstructed horizontal surface over both urban and mountainous areas. The diurnal
15 variation of direct flux is very similar to that of the total flux, which has been illustrated in
16 detail in the last section. In general, deviations in diffuse flux (plus coupled flux) are negative
17 over both urban and mountainous areas since sky view factors are less than 1.0 in street
18 canyons or valleys. Their magnitude is generally between -0.03 W m^{-2} and -0.10 W m^{-2} in
19 typical urban areas in Domain 1 (Fig. 5b, Fig. S3) and between -0.10 W m^{-2} and -0.25 W m^{-2}
20 in typical urban areas in Domain 2 (Fig. 5c), both peaking at noon. Deviations in direct-
21 reflected and diffuse-reflected fluxes are always positive because these two components do
22 not exist on unobstructed horizontal surfaces. The magnitude of direct-reflected flux ranges
23 between $0.01\text{--}0.20 \text{ W m}^{-2}$ in typical urban areas (both Domain 1 and Domain 2), with peaks
24 occurring at summer noon. Figure S3 shows that deviations in the direct-reflected flux can
25 exceed those of the direct flux for a few hours around summer noon. The magnitude of the
26 diffuse-reflected flux is always negligible compared with the components described above.

27 **3.3 Sensitivity analysis**

28 **3.3.1 Effect of aerosols on flux deviations**

29 In preceding discussions, we focused on the effect of buildings in clear-sky condition without
30 aerosols. Atmospheric aerosols can potentially alter the transfer of solar radiation. As
31 described in Section 2.2, although the 3-D radiation parameterization was developed in clear-



1 sky condition without aerosols, regression equations for F'_{dir} and F'_{rdir} can be directly applied
2 to aerosol contaminated environment, while those for F'_{dif} , F'_{rdif} , and F'_{coup} can provide a first-
3 order estimate. Figure 2 shows hourly flux deviations between 3-D and plane-parallel at
4 selected times (7:00, 12:00, and 17:00 BT) on April 1st with and without aerosols. The results
5 on the other simulation days (January 1st, July 1st, and October 1st) are quite similar, and thus
6 are now shown. In general, the inclusion of aerosols reduces the magnitude of surface flux
7 deviations without changing the spatial pattern. This can be explained by the attenuation of
8 total solar fluxes by aerosols across the domain. Over the urban center (Domain 2), aerosols
9 reduce the magnitude of daily average deviations by about 15–30%. The reduction ratios are
10 significantly higher in the early morning and late afternoon (40–65%) than at noon (10–25%),
11 mainly due to higher aerosol optical depths in the early morning/late afternoon. In this study,
12 interactions between buildings and aerosols are not considered in the simulation. For example,
13 photons reflected by buildings can further be scattered/absorbed by aerosols, and vice versa.
14 Given that diffuse-reflected and coupled fluxes are much smaller than direct flux, the resulting
15 errors should be minor. The 3-D Monte Carlo photon tracing program is needed in order to
16 achieve a more accurate evaluation of the effect of aerosols on flux deviations.

17 3.3.2 Sensitivity of flux deviations to spatial resolutions

18 As demonstrated in Section 3.1, the magnitude of flux deviations from the flat surface is quite
19 sensitive to spatial resolutions. Over urban areas, hourly deviations are $\pm 1\text{--}10\text{ W m}^{-2}$ at 800-m
20 resolution and within $\pm 1\text{ W m}^{-2}$ at 4-km resolution. The smaller values in coarser grids can be
21 explained by the compensation effect of positive and negative deviations on the opposite side
22 of buildings. Judging from the right panel of Fig. 1, an $800\times 800\text{ m}^2$ grid still covers quite a
23 few buildings, which motivates us to explore the potential effect of buildings at even finer
24 resolutions. As a test case, we present a rough estimate of flux deviations at a 3 arc-second
25 (about 90 m) resolution (shown in Fig. 6) by applying the 3-D radiation parameterization to 3
26 arc-second topography data derived from SRTM. Theoretically, the parameterization may not
27 be applicable to a spatial resolution less than about 1 km with acceptable accuracy.
28 Nevertheless, it suffices to provide an initial estimate for flux deviations, though results must
29 be interpreted with care. Of course, a more accurate estimation should be made using the
30 Monte Carlo method in future studies. Figure 6 shows that hourly deviations in 90 m grids are
31 generally between $\pm 5\text{--}50\text{ W m}^{-2}$, and the maximum local deviations can reach about ± 100



1 W m^{-2} . This is notably higher than flux deviations at 800-m resolution. These results highlight
2 the potential importance of 3-D building effects on the microscale modeling with resolutions
3 of 1–100 m (e.g., urban dispersion models), which requires further studies.

4 3.3.3 Sensitivity of flux deviations to the surface albedo

5 The surface albedo used in the 3-D radiation parameterization was directly derived from
6 WRF/CMAQ simulation results, which ranges between 0.15–0.20 and represents the typical
7 surface albedo of urban areas. However, there is a wide variety of roofing materials with
8 distinct albedos (Prado and Ferreira, 2005). One geoengineering proposal to ameliorate the
9 effect of urban heat island was to use reflective roofing material or to paint existing roofs
10 white (Jacobson and Ten Hoeve, 2012). There are also increasing numbers of buildings with
11 glass surfaces. To evaluate the potential effect of amplified surface albedo on flux deviations
12 from the horizontal surface, we design three sensitivity cases in which domain-wide surface
13 albedo was uniformly increased to 0.35, 0.50, and 0.65. Figure 7 shows simulated surface
14 solar flux deviations in a typical urban area in Domain 1 (defined as rectangle B in Fig. 1) as a
15 function of surface albedo. We focus on urban areas in Domain 1 (4-km resolution) because it
16 is the region where the largest relative contribution of the reflected flux is identified (see Fig.
17 5), implying a potentially large sensitivity to surface albedo. Figure 7 shows a moderate
18 impact of surface albedo on flux deviations during the day. The largest sensitivity occurs at
19 summer noon, at which a large albedo of 0.65 can amplify flux deviations from 0.1–0.4 W m^{-2}
20 to about 0.6 W m^{-2} . Compared with the case of a 4-km resolution, the change in surface
21 albedo results in a much smaller relative change in flux deviations at 800-m resolution,
22 because the relative contribution of the reflected flux is smaller at 800-m resolution (see Fig.
23 5).

24 3.4 Implications for atmospheric studies

25 The present results have important implication for future studies. Deviations in surface solar
26 fluxes are within 1 W m^{-2} at a 4 km or coarser resolution due to the offset of positive and
27 negative flux deviations, therefore the effect of buildings may not be critically significant in
28 mesoscale atmospheric models. Nevertheless, the effect can not be neglected if there is a
29 substantially inhomogeneous subgrid-scale distribution of plants, accumulated snow, and
30 building/road materials, etc.; in this case, subgrid-scale flux deviations may result in biased
31 evapotranspiration, snowmelting, and heat fluxes, etc. For meso-urban models with a typical



1 resolution of about 1 km (e.g., urbanized MM5 model, uMM5; Taha et al., 2008), the 3-D
2 building effects become quite significant (about $\pm 1\text{--}10\text{ W m}^{-2}$). The parameterization used in
3 this study can be readily incorporated in these models to account for 3-D building effects. As
4 for computational fluid dynamics models (e.g., FLUENT) and urban dispersion models (e.g.,
5 Atmospheric Dispersion Modelling System, ADMS) with resolutions of 1–100 m, this study
6 implies that flux deviations induced by buildings might be up to $\pm 100\text{ W m}^{-2}$. The large flux
7 deviations can significantly alter local energy balance, and thus affects the spatial distribution
8 of temperature and small-scale flows around buildings and/or through street canyons.
9 Therefore, the 3-D building effects on solar fluxes can play a crucial role in numerical
10 simulation of urban meteorology and air pollutant dispersion. The present 3-D radiation
11 parameterization may not be applicable to 1–100 m resolutions. As such, a more physically-
12 based approach directly using an appropriate 3-D Monte Carlo photon tracing program will be
13 needed to account for 3-D building effects more precisely. Also, topography data such as the
14 recently released SRTM datasets at a resolution of 1 arc-second (about 30 m) may also be
15 useful for the study of 3-D building effects.

16 **4 Conclusions**

17 In this study, we systematically evaluated the impact of buildings on surface solar fluxes over
18 urban Beijing using the 3-D radiation parameterization developed in our previous study in
19 connection with the FLG radiative transfer scheme. The evaluation was conducted in two
20 simulation domains with grid resolutions of 4 km and 800 m, representing typical resolutions
21 for mesoscale and meso-urban models, respectively.

22 Over urban Beijing, deviations in surface solar fluxes between the 3-D radiation
23 parameterization and the plane-parallel scheme are generally $\pm 1\text{--}10\text{ W m}^{-2}$ at 800-m
24 resolution and within $\pm 1\text{ W m}^{-2}$ at 4-km resolution. Pairs of positive-negative flux deviations
25 on different sides of buildings are resolved at 800-m resolution, while they offset each other at
26 4-km resolution. Deviations in surface solar fluxes over urban areas are considerably smaller
27 than those over mountainous areas using preceding grid resolutions.

28 Flux deviations over urban areas are positive around noon but negative in the early morning
29 and late afternoon at 4-km resolution. The corresponding deviations at 800-m resolution, in
30 contrast, show diurnal variations that are strongly dependent on the grids' relative locations to
31 buildings. Both the magnitude and spatiotemporal variations of flux deviations are largely
32 dominated by the direct flux.



1 With a series of sensitivity simulations, we show that atmospheric aerosols reduce the
2 magnitude of surface flux deviations by 10–65% without changing the spatial pattern.
3 Simulated deviations in surface fluxes are very sensitive to spatial resolution. They can
4 potentially reach up to $\pm 100 \text{ W m}^{-2}$ at a high resolution of about 90 m. The surface albedo has
5 a moderate impact on flux deviations during the day, while the impact can be substantial at
6 summer noon.

7 This study implies that the effect of buildings on surface solar fluxes may not be critically
8 important in mesoscale atmospheric models ($\geq 4\text{-km}$ resolution). However, the effect can play
9 a crucial role in meso-urban atmospheric models as well as microscale urban dispersion
10 models with resolutions of 1 m – 1 km.

11

12

13 **Acknowledgments.** This research was supported by the NSF under grant AGS-0946315
14 and AGS-1523296. LRL was supported by Department of Energy Office of Science
15 Biological and Environmental Research through the Regional and Global Climate Modeling
16 program. PNNL is operated for DOE by Battelle Memorial Institute under contract DE-AC05-
17 76RL01830.

18

19

20 References

- 21 Chen, Y., Hall, A., and Liou, K. N.: Application of three-dimensional solar radiative transfer
22 to mountains, *J Geophys Res-Atmos*, 111, D21111, DOI 10.1029/2006jd007163, 2006.
- 23 Dozier, J., and Frew, J.: Rapid calculation of terrain parameters for radiation modeling from
24 digital elevation data, *Ieee T Geosci Remote*, 28, 963-969, Doi 10.1109/36.58986, 1990.
- 25 Dubayah, R., Dozier, J., and Davis, F. W.: Topographic distribution of clear-sky radiation
26 over the konza prairie, kansas, *Water Resour Res*, 26, 679-690, Doi 10.1029/89wr03107,
27 1990.
- 28 Essery, R., and Marks, D.: Scaling and parametrization of clear-sky solar radiation over
29 complex topography, *J Geophys Res-Atmos*, 112, D10122, DOI 10.1029/2006jd007650,
30 2007.
- 31 Fu, Q., and Liou, K. N.: On the correlated k-distribution method for radiative-transfer in
32 nonhomogeneous atmospheres, *J Atmos Sci*, 49, 2139-2156, Doi 10.1175/1520-
33 0469(1992)049<2139:Otcdfm>2.0.Co;2, 1992.
- 34 Grimmond, C. S. B., Blackett, M., Best, M. J., Barlow, J., Baik, J. J., Belcher, S. E.,
35 Bohnenstengel, S. I., Calmet, I., Chen, F., Dandou, A., Fortuniak, K., Gouvea, M. L.,
36 Hamdi, R., Hendry, M., Kawai, T., Kawamoto, Y., Kondo, H., Krayenhoff, E. S., Lee, S.
37 H., Loridan, T., Martilli, A., Masson, V., Miao, S., Oleson, K., Pigeon, G., Porson, A., Ryu,



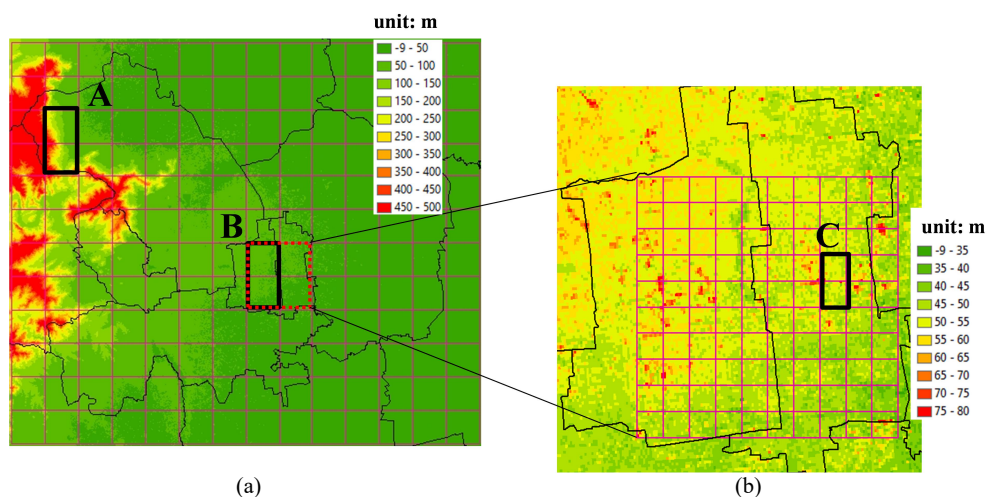
- 1 Y. H., Salamanca, F., Shashua-Bar, L., Steeneveld, G. J., Tombrou, M., Voogt, J., Young,
2 D., and Zhang, N.: The international urban energy balance models comparison project: First
3 results from phase 1, *J Appl Meteorol Clim*, 49, 1268-1292, 10.1175/2010JAMC2354.1,
4 2010.
- 5 Grimmond, C. S. B., Blackett, M., Best, M. J., Baik, J. J., Belcher, S. E., Beringer, J.,
6 Bohnenstengel, S. I., Calmet, I., Chen, F., Coutts, A., Dandou, A., Fortuniak, K., Gouvea,
7 M. L., Hamdi, R., Hendry, M., Kanda, M., Kawai, T., Kawamoto, Y., Kondo, H.,
8 Krayenhoff, E. S., Lee, S. H., Loridan, T., Martilli, A., Masson, V., Miao, S., Oleson, K.,
9 Ooka, R., Pigeon, G., Porson, A., Ryu, Y. H., Salamanca, F., Steeneveld, G. J., Tombrou,
10 M., Voogt, J. A., Young, D. T., and Zhang, N.: Initial results from phase 2 of the
11 international urban energy balance model comparison, *Int J Climatol*, 31, 244-272,
12 10.1002/joc.2227, 2011.
- 13 Gu, Y., Farrara, J., Liou, K. N., and Mechoso, C. R.: Parameterization of cloud-radiation
14 processes in the ucla general circulation model, *J Climate*, 16, 3357-3370, Doi
15 10.1175/1520-0442(2003)016<3357:Pocpit>2.0.Co;2, 2003.
- 16 Gu, Y., Liou, K. N., Xue, Y., Mechoso, C. R., Li, W., and Luo, Y.: Climatic effects of
17 different aerosol types in china simulated by the ucla general circulation model, *J Geophys*
18 *Res-Atmos*, 111, D15201, DOI 10.1029/2005jd006312, 2006.
- 19 Gu, Y., Liou, K. N., Chen, W., and Liou, H.: Direct climate effect of black carbon in china
20 and its impact on dust storms *JOURNAL OF GEOPHYSICAL RESEARCH:*
21 *ATMOSPHERES*, 115, D00K14, DOI 10.1029/2009JD013427, 2010.
- 22 Gu, Y., Liou, K. N., Lee, W. L., and Leung, L. R.: Simulating 3-d radiative transfer effects
23 over the sierra nevada mountains using wrf, *Atmos Chem Phys*, 12, 9965-9976,
24 10.5194/acp-12-9965-2012, 2012.
- 25 Heald, C. L.: Geos-chem aerosol optics, available at
26 http://www.Atmos.Colostate.Edu/~heald/docs/geos_chem_optics_description.Pdf, 2010.
- 27 Iwabuchi, H., and Kobayashi, H.: Modeling of radiative transfer in cloudy atmospheres and
28 plant canopies using monte carlo methods. Frcgc technical report 8, 2008.
- 29 Jacobson, M. Z., and Ten Hoeve, J. E.: Effects of urban surfaces and white roofs on global
30 and regional climate, *J Climate*, 25, 1028-1044, 10.1175/Jcli-D-11-00032.1, 2012.
- 31 Jarvis, A., Reuter, H. I., Nelson, A., and Guevara, E.: Hole-filled seamless srtm data v4,
32 available at <http://srtm.Csi.Cgiar.Org>, International Centre for Tropical Agriculture, 2008.
- 33 Kondo, H., Genchi, Y., Kikegawa, Y., Ohashi, Y., Yoshikado, H., and Komiyama, H.:
34 Development of a multi-layer urban canopy model for the analysis of energy consumption
35 in a big city: Structure of the urban canopy model and its basic performance, *Bound-Lay*
36 *Meteorol*, 116, 395-421, 10.1007/s10546-005-0905-5, 2005.
- 37 Kusaka, H., Kondo, H., Kikegawa, Y., and Kimura, F.: A simple single-layer urban canopy
38 model for atmospheric models: Comparison with multi-layer and slab models, *Bound-Lay*
39 *Meteorol*, 101, 329-358, Doi 10.1023/A:1019207923078, 2001.
- 40 Kusaka, H., and Kimura, F.: Coupling a single-layer urban canopy model with a simple
41 atmospheric model: Impact on urban heat island simulation for an idealized case, *J*
42 *Meteorol Soc Jpn*, 82, 67-80, Doi 10.2151/Jmsj.82.67, 2004.
- 43 Lai, Y. J., Chou, M. D., and Lin, P. H.: Parameterization of topographic effect on surface solar
44 radiation, *J Geophys Res-Atmos*, 115, D01104, DOI 10.1029/2009jd012305, 2010.
- 45 Lee, W. L., Liou, K. N., and Hall, A.: Parameterization of solar fluxes over mountain surfaces
46 for application to climate models, *J Geophys Res-Atmos*, 116, D01101, DOI
47 10.1029/2010jd014722, 2011.



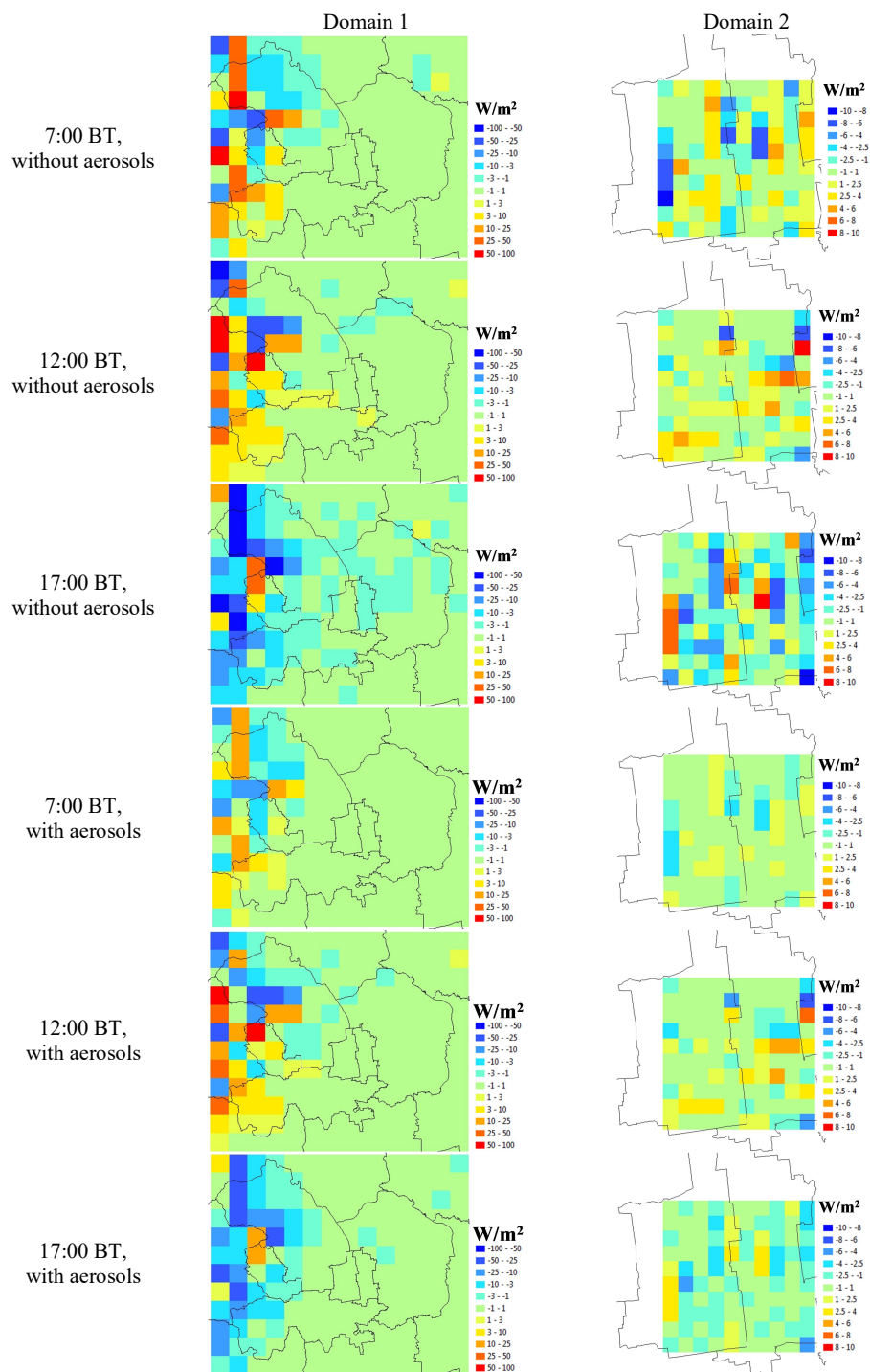
- 1 Lee, W. L., Liou, K. N., and Wang, C. C.: Impact of 3-d topography on surface radiation
2 budget over the tibetan plateau, *Theor Appl Climatol*, 113, 95-103, 10.1007/s00704-012-
3 0767-y, 2013.
- 4 Lee, W. L., Gu, Y., Liou, K. N., Leung, L. R., and Hsu, H. H.: A global model simulation for
5 3-d radiative transfer impact on surface hydrology over the sierra nevada and rocky
6 mountains, *Atmos Chem Phys*, 15, 5405-5413, 10.5194/acp-15-5405-2015, 2015.
- 7 Liou, K. N., Lee, W. L., and Hall, A.: Radiative transfer in mountains: Application to the
8 tibetan plateau, *Geophys Res Lett*, 34, L23809, DOI 10.1029/2007gl031762, 2007.
- 9 Liou, K. N., Gu, Y., Leung, L. R., Lee, W. L., and Fovell, R. G.: A wrf simulation of the
10 impact of 3-d radiative transfer on surface hydrology over the rocky mountains and sierra
11 nevada, *Atmos Chem Phys*, 13, 11709-11721, 10.5194/acp-13-11709-2013, 2013.
- 12 Martin, R., and Heald, C. L.: Aerosol optical properties update for geos-chem v8-03-01,
13 available at http://wiki.Seas.Harvard.Edu/geos-chem/index.Php/aerosol_optical_properties,
14 2010.
- 15 Mayer, B., Hoch, S. W., and Whiteman, C. D.: Validating the mystic three-dimensional
16 radiative transfer model with observations from the complex topography of arizona's
17 meteor crater, *Atmos Chem Phys*, 10, 8685-8696, 10.5194/acp-10-8685-2010, 2010.
- 18 Oleson, K. W., Bonan, G. B., Feddema, J., Vertenstein, M., and Grimmond, C. S. B.: An
19 urban parameterization for a global climate model. Part i: Formulation and evaluation for
20 two cities, *J Appl Meteorol Clim*, 47, 1038-1060, 10.1175/2007JAMC1597.1, 2008.
- 21 Prado, R. T. A., and Ferreira, F. L.: Measurement of albedo and analysis of its influence the
22 surface temperature of building roof materials, *Energ Buildings*, 37, 295-300,
23 10.1016/j.enbuild.2004.03.009, 2005.
- 24 Preisendorfer, R. W., and Mobley, C. D.: Albedos and glitter patterns of a wind-roughened
25 sea-surface, *J Phys Oceanogr*, 16, 1293-1316, Doi 10.1175/1520-
26 0485(1986)016<1293:Aagpoa>2.0.Co;2, 1986.
- 27 Taha, H.: Episodic performance and sensitivity of the urbanized mm5 (umm5) to
28 perturbations in surface properties in houston texas, *Bound-Lay Meteorol*, 127, 193-218,
29 10.1007/s10546-007-9258-6, 2008.
- 30
31



1 Tables and figures

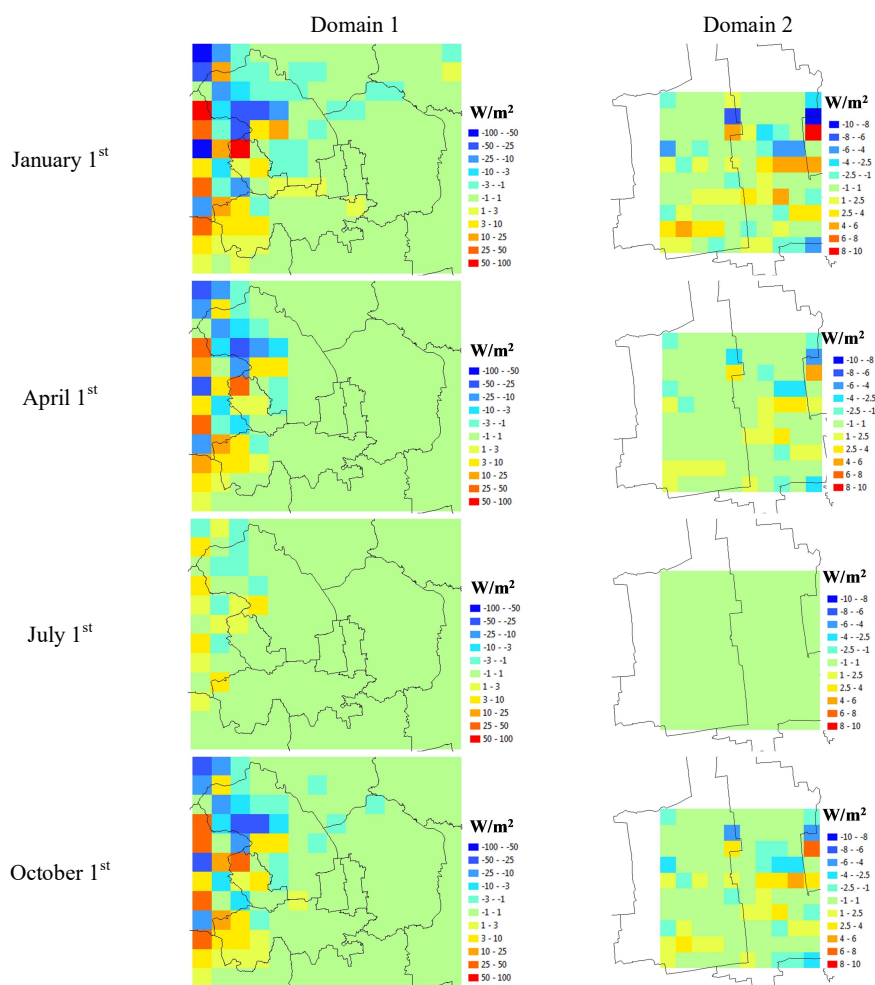


- 2 Figure 1. Modelling domains used in 3-D radiative transfer calculation: (a) Domain 1
3 covering urban and suburban Beijing at a grid resolution of 4 km; (b) Domain 2 covering the
4 urban center of Beijing at a grid resolution of 800 m. The colours represent altitudes at a
5 resolution of 3 arc-second (about 90 m) derived from SRTM. The black thin lines represent
6 boundaries of districts. The three black bold rectangles (defined as A, B, and C, respectively)
7 represent typical grids used to analyze diurnal variation and to quantify the contribution of
8 flux components. The red dashed rectangle represents grids in Domain 1 that correspond to
9 Domain 2.
10

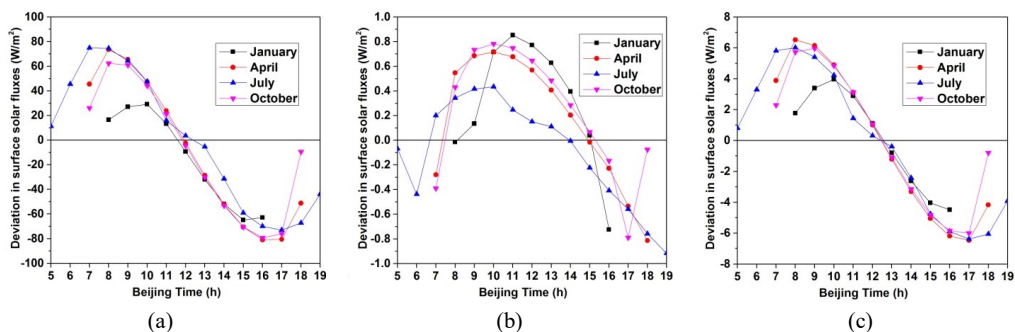




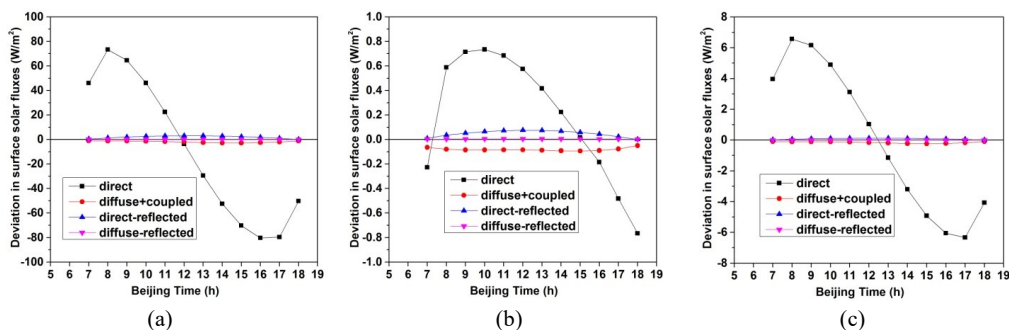
1 Figure 2. Surface solar flux deviations between the 3-D radiation parameterization and the
2 plane-parallel scheme at selected times (7:00, 12:00, and 17:00 BT) on April 1st in conditions
3 with and without aerosols.
4



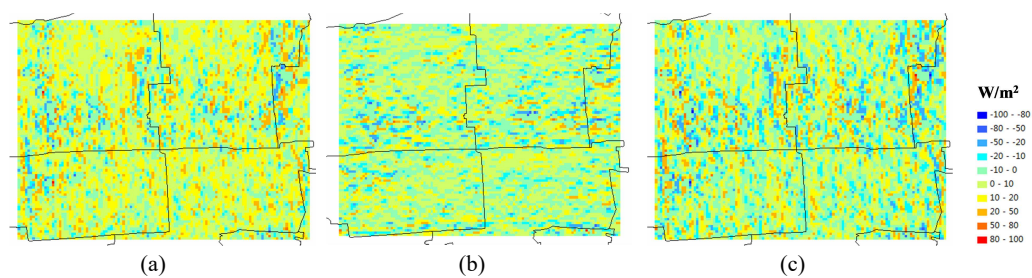
5 Figure 3. Daily average surface solar flux deviations between the 3-D radiation
6 parameterization and the plane-parallel scheme in clear-sky condition without aerosols on
7 January 1st, April 1st, July 1st, and October 1st, 2012.
8



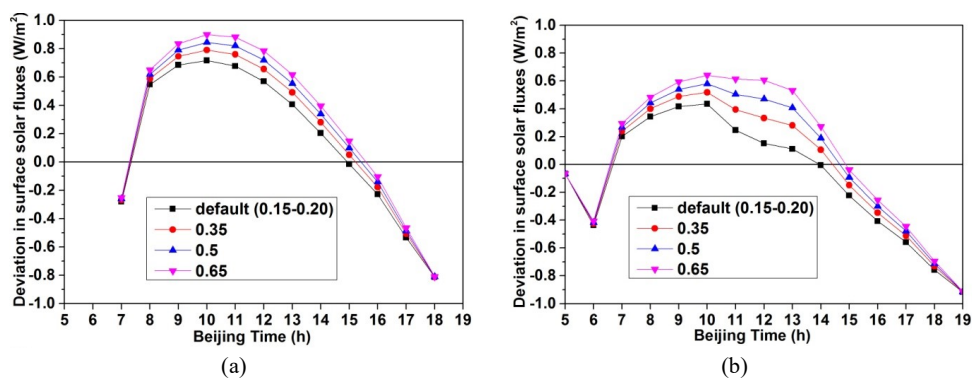
1 Figure 4. Diurnal variation of surface solar flux deviations between the 3-D radiation
2 parameterization and the plane-parallel scheme in clear-sky condition without aerosols in
3 typical grids marked by black bold rectangles in Fig. 1: (a) a typical mountainous area,
4 defined as rectangle A; (b) a typical urban area in Domain 1, defined as rectangle B; (c) a
5 typical urban area in Domain 2, defined as rectangle C.
6



1 Figure 5. Contributions of individual components to surface solar flux deviations between the
2 3-D radiation parameterization and the plane-parallel scheme in clear-sky condition without
3 aerosols in typical grids on April 1st. Panel (a), (b), and (c) are for the same grids as Fig. 4(a),
4 Fig. 4(b), and Fig. 4(c).
5



1 Figure 6. Surface solar flux deviations between the 3-D radiation parameterization and the
2 plane-parallel scheme on April 1st at a grid resolution of 3 arc-second (about 90 m). (a) 7:00
3 BT; (b) 12:00 BT; (c) 17:00 BT. The size of the simulation domain is the same as Domain 2
4 defined in Fig. 1.
5



1 Figure 7. Sensitivity of surface solar flux deviations between the 3-D radiation
2 parameterization and the plane-parallel scheme to the surface albedo in a typical urban area in
3 Domain 1 (defined as rectangle B in Fig. 1) on (a) April 1st, (b) July 1st.